ANL-6501

ANL-6501

Copy 1

Argonne National Laboratory

SOME CALCULATIONS PERTAINING TO FAST REACTOR SAFETY

by

D. M. O'Shea, D. Okrent,
and J. M. Chaumont

ANL-6501
Reactor Technology
(TID-4500, 17th Ed.)
AEC Research and
Development Report

ARGONNE NATIONAL LABORATORY
9700 South Cass Avenue
Argonne, Illinois

SOME CALCULATIONS PERTAINING TO FAST REACTOR SAFETY

by

D. M. O'Shea, D. Okrent, and J. M. Chaumont*
Reactor Engineering Division

February 1962

*On loan from Commissariat a l'Energie Atomique, Paris, France

Operated by The University of Chicago
under
Contract W-31-109-eng-38

TABLE OF CONTENTS

LIST OF FIGURES

LIST OF FIGURES

LIST OF TABLES

SOME CALCULATIONS PERTAINING TO FAST REACTOR SAFETY

by

D. M. O'Shea, D. Okrent, and J. M. Chaumont

PREFACE

The general program in fast reactor safety at Argonne National Laboratory includes both experimental and theoretical work. As part of the latter aspect, techniques and accuracy of calculation, as well as the safety predictions thereof, are considered. A pair of preliminary studies of such a nature form the heart of this report.

The first topic deals with the surprising success obtained in analyzing complicated meltdown configurations using two-dimensional, two-group diffusion theory. The second topic deals with the dependence of energy yield in a fast reactor explosion on the shape of the power distribution in the core.

In addition, the results of a brief survey dealing with the change of dynamic reactor behavior during various startup accidents as a consequence of a reduction in the delayed-neutron fraction are summarized.

I. MELTDOWN CONFIGURATIONS

A. Introduction

One of the major problems of nuclear safety in fast power reactors is related to core meltdown.[1] The presence of many critical masses of fissionable material within a single, low-fuel-density, fast power reactor provides a considerable potential for large reactivity increases, should meltdown lead to a significant increase in the effective fuel density. Actually, the most crucial factor in determining the energy developed in a nuclear burst is not the total reactivity available, but the rate at which it is added. This dynamic quantity is sensitive to a great many variables, making it extremely difficult to ascertain.

However, it is also of interest to determine the degree to which one can calculate the static properties of such configurations. Things like power distributions and critical mass fall into this category. If one is also given curves of the reactivity worth of core materials, i.e., danger coefficients as a function of position, it becomes possible to perform fairly simple

calculations of the reactivity changes during the initial portions of a burst by means of two-dimensional geometry. This latter calculation is of specific interest in investigations of autocatalytic effects in explosions. It is important to learn whether any peculiar geometric arrangements might occur wherein the early motions of the fuel due to pressure buildup during a burst lead to a gain, rather than a loss, in reactivity.

For all these reasons, a pair of hypothetical meltdown configurations for the Enrico Fermi reactor were assembled and studied at Argonne's ZPR-III fast critical facility. The experimental results have been reported in part elsewhere.[2] Such experiments are time-consuming, and hence must be limited in number. However, the availability of measurements for two such assemblies provides a good basis for testing theoretical techniques for predicting the experimental data.

As the simplest technique that afforded a chance of giving decent results, two-dimensional, two-group diffusion theory[3] was used to predict these experiments. Theory and experiment are compared herein for critical mass, power distribution, and danger coefficients; the calculating technique was actually fully specified in advance of experiment. No adjustments have been made after the comparison to improve agreement.

A comparison of experiment with the predictions of two-dimensional transport theory[4] for power distributions was also made.

B. Calculation Details

1. Adaptation of the PDQ Code

The PDQ code does not include the option of calculating the adjoint flux. Some transformations of the input quantities were necessary in order to make the code compute an adjoint solution,[5] and, since PDQ does not allow any fission neutrons to be born in the last group, the two-group calculations were obliged to carry a third dummy group. The revised form was as follows:

$$\nabla D_1 \nabla \Phi_1 - \Sigma_1^a \Phi_1 - \Sigma_1^R \Phi_1 + \frac{\chi_1}{\lambda} \left(\nu_1 \Sigma_1^f \Phi_1 + \nu_2 \Sigma_2^f \Phi_2 \right) = 0$$

$$\nabla D_2 \nabla \Phi_2 - \Sigma_2^a \Phi_2 + \Sigma_1^R \Phi_1 + \frac{\chi_2}{\lambda} \left(\nu_1 \Sigma_1^f \Phi_1 + \nu_2 \Sigma_2^f \Phi_2 \right) = 0 \qquad (1)$$

$$\nabla D_3 \nabla \Phi_3 = 0 \quad .$$

The equations for the adjoint problem are

$$\nabla D_3 \nabla \Phi_3^* = 0$$

$$\nabla D_2 \nabla \Phi_2^* - \Sigma_2^a \Phi_2^* + \frac{\nu_2 \Sigma_2^f}{\lambda} \left(\chi_1 \Phi_1^* + \chi_2 \Phi_2^* \right) = 0 \qquad (2)$$

$$\nabla D_1 \nabla \Phi_1^* - \left(\Sigma_1^a + \Sigma_1^R \right) \Phi_1^* + \Sigma_1^R \Phi_2^* + \frac{\nu_1 \Sigma_1^f}{\lambda} \left(\chi_1 \Phi_1^* + \chi_2 \Phi_2^* \right) = 0 \quad ,$$

which can be written as

$$\nabla D_3 \nabla \Phi_3^* = 0$$

$$\nabla D_2 \nabla \Phi_2^* - \left(\Sigma_2^a - \Sigma_1^R - \frac{\nu_1 \Sigma_1^f}{\lambda} \chi_2 \right) \Phi_2^* - \left(\Sigma_1^R + \frac{\nu_1 \Sigma_1^f}{\lambda} \chi_2 \right) \Phi_2^*$$

$$+ \frac{1}{\lambda} \left(\chi_1 \nu_2 \Sigma_2^f \Phi_1^* + \chi_2 \nu_2 \Sigma_2^f \Phi_2^* \right) = 0 \qquad (3)$$

$$\nabla D_1 \nabla \Phi_1 - \left(\Sigma_1^a + \Sigma_1^R - \frac{\nu_1 \Sigma_1^f}{\lambda} \chi_1 \right) \Phi_1^* + \left(\Sigma_1^R + \frac{\nu_1 \Sigma_1^f}{\lambda} \chi_2 \right) \Phi_2^* = 0 \quad .$$

The transformations for two groups are:

For	Substitute
Φ_1	Φ_3^* (Dummy)
Φ_2	Φ_2^*
Φ_3	Φ_1^*
D_1	D_3
D_2	D_2
D_3	D_1

For	Substitute
Σ_1^a	0
Σ_2^a	$\Sigma_2^a - \Sigma_1^R - \frac{\nu_1 \Sigma_1^f}{\lambda} \chi_2$
Σ_3^a	$\Sigma_1^a + \Sigma_1^R - \frac{\nu_1 \Sigma_1^f}{\lambda} \chi_1$
Σ_1^R	0
Σ_2^R	$\Sigma_1^R + \frac{\nu_1 \Sigma_1^f}{\lambda} \chi_2$

For	Substitute
$\nu_1 \Sigma_1^f$	0
$\nu_2 \Sigma_2^f$	$\nu_2 \Sigma_2^f \chi_2$
$\nu_3 \Sigma_3^f$	$\nu_2 \Sigma_2^f \chi_1$
χ_1	0
χ_2	1
χ_3	0

2. Danger Coefficients

The danger coefficients of different materials were calculated by a perturbation formula, which in the two-group case was

$$\frac{\Delta K}{K} = \frac{1}{F}\Big\{ - \delta D_1 \nabla\phi_1 \nabla\phi_1^* - \delta D_2 \nabla\phi_2 \nabla\phi_2^* - \delta\Sigma_1^a \phi_1 \phi_1^* - \delta\Sigma_2^a \phi_2 \phi_2^* + (\phi_2^* - \phi_1^*)\, \delta\Sigma_1^R \phi_1$$

$$+ (\chi_1 \phi_1^* + \chi_2 \phi_2^*) \left[\left(\delta\nu\Sigma_1^f \right) \phi_1 + \delta\left(\nu\Sigma_2^f \right) \phi_2 \right] \Big\} \quad , \tag{4}$$

in which F is a normalization factor:

$$F = \int_{\substack{\text{Over} \\ \text{all the} \\ \text{Reactor}}} dV \left(\chi_1 \phi_1^* + \chi_2 \phi_2^* \right) \left(\nu\Sigma_1^f \phi_1 + \nu\Sigma_2^f \phi_2 \right) \quad .$$

The quantities $\delta\Sigma^a$, $\delta\Sigma^R$, and $\delta\nu\Sigma^F$ can be taken equal to the homogeneous cross-section changes of the material. Also,

$$\delta D = - 3 D_0 \delta\Sigma_{tr} \quad ,$$

with D_0 the diffusion coefficient of the region and $\delta\Sigma_{tr}$ the transport cross section of the material.

3. Neutron Cross Sections

A set of two-group cross sections was obtained by collapsing the eleven-group set of Loewenstein and Okrent.[6] The eleven-group constants were averaged with the aid of the eleven-group calculated flux spectrum for a reactor similar in composition to that of the Enrico Fermi reactor. These two-group cross sections were then used in PDQ to make a calculation for ZPR-III Assembly 20, which was a mockup of the Fermi reactor in its normal configuration. The result of the calculation was a somewhat subcritical reactor. The value of ν for U^{235} was then arbitrarily adjusted about 2% to give agreement between measured and calculated critical mass for this one assembly. The adjusted two-group cross sections are listed in Table I.

Table I

TWO-GROUP CROSS SECTIONS

	Group	E_L(mev)	χ	σ_f	σ_c	$\nu\Sigma_f$	σ_R	σ_{tr}
U^{235}	1	1.35	0.574	1.3	0.1	3.518	1.4	4.7
($N = 0.048 \times 10^{24}$)	2	-	0.426	1.4	0.3	3.574	-	6.0
U^{238}	1			0.53	0.04	1.484	2.1	4.7
($N = 0.048 \times 10^{24}$)	2			-	0.18	-	-	7.0
Fe	1			-	0.0025	-	0.74	2.1
($N = 0.085 \times 10^{24}$)	2			-	0.0057	-	-	2.9
Al	1			-	0.0003	-	0.38	1.8
($N = 0.060 \times 10^{24}$)	2			-	0.0024	-	-	3.0
Mo	1			-	0.02	-	1.06	3.0
($N = 0.064 \times 10^{24}$)	2			-	0.055	-	-	6.38

C. First Meltdown Configuration

1. Description

In the first meltdown configuration, a central section of the Fermi core is assumed to have melted and settled at the bottom to form a region of dense core material. The space above this region is then left as nearly void.

This configuration was assembled as Assembly No. 27 of ZPR-III. A sketch of the system along with its associated dimensions appears in Fig. 1. The compositions of the various regions are given in Table II. The stainless steel and zirconium were combined and treated as iron in the calculation.

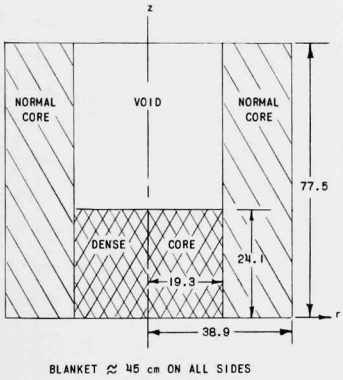

Fig. 1

First Meltdown Configuration: ZPR-III Assembly No. 27. All Dimensions in Centimeters

Table II

REGIONAL VOLUME FRACTIONS, %

	U^{238}	U^{235}	Al	Stainless Steel	Mo	Zr
Normal Core Region	17.16	6.04	27.81	16.90	5.18	4.41
Dense Core Region	42.56	14.80	-	14.50	15.50	4.98
Void Region	-	-	4.22	9.32		
Blanket	48.70	0.11	13.47	21.0		

2. Critical Mass and Fission Rate

The PDQ calculation led to a prediction of 393.5 kg for the critical mass, which may be compared with the experimental value of 390.9 kg. The agreement was surprising, almost amazing.

The calculated rate of fission for U^{235} for radial traverses across the dense core region and across the void region is compared with the experimental value in Fig. 2. The results of the PDQ calculation have been normalized to the experimental values at the center of the dense core region. The agreement in both cases is fairly good.

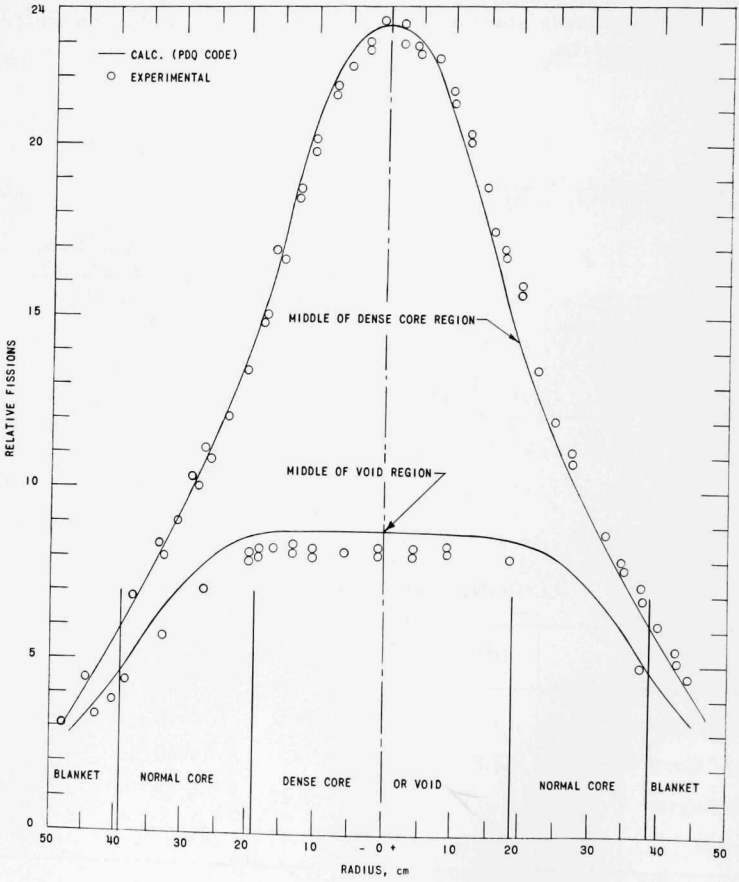

Fig. 2. Radial Distribution of U^{235} Fissions for the First Meltdown Configuration

The calculated fission rate along the axial centerline is compared with the experimental results in Fig. 3. The agreement is less good in that the slope of the PDQ distribution differs somewhat from that shown by experiment for the void region. A calculation by means of the TDC transport code was done for this configuration, and the results for the axial fission rate are plotted as a dashed curve in Fig. 3. The agreement in slope across the void region is better in this case.

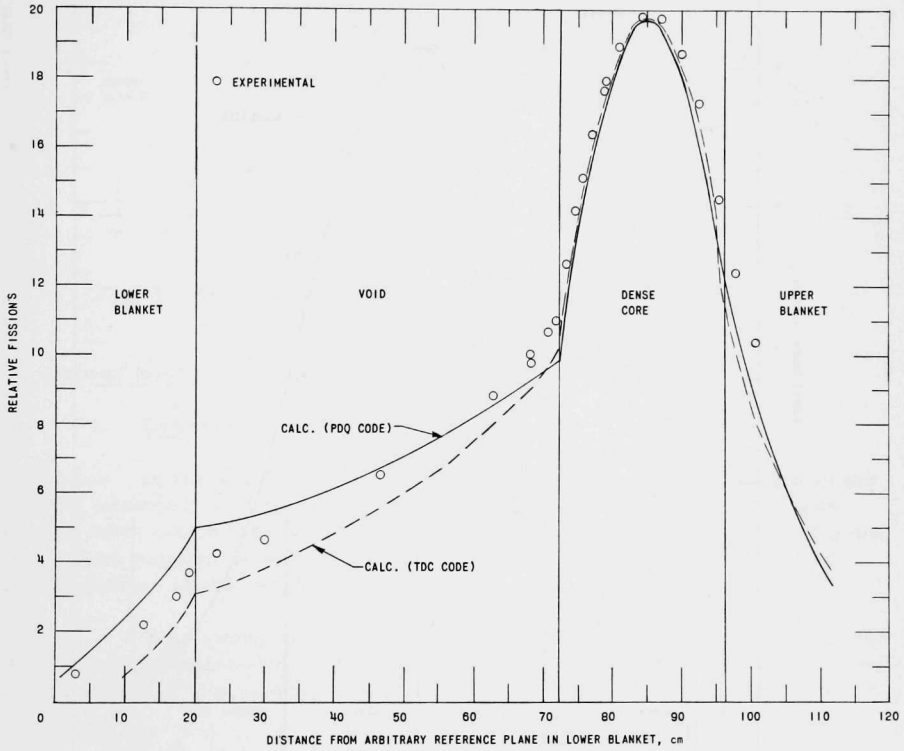

Fig. 3. Axial Distribution of U^{235} Fissions for the First Meltdown Configuration

3. Danger Coefficient Distribution

The danger coefficient for a dense core sample was calculated from Eq. (4) by means of the fluxes from the PDQ code. Because of the considerable amount of work involved in evaluating the normalization factor F in Eq. (4) by hand, this factor was not computed. Instead, the danger coefficient was normalized to the experimental value at the center of the dense core region.

The danger coefficient distributions for a radial traverse across the middle of the dense core and an axial traverse along the axial centerline are given in Figs. 4 and 5, respectively. The agreement in both cases is fairly good.

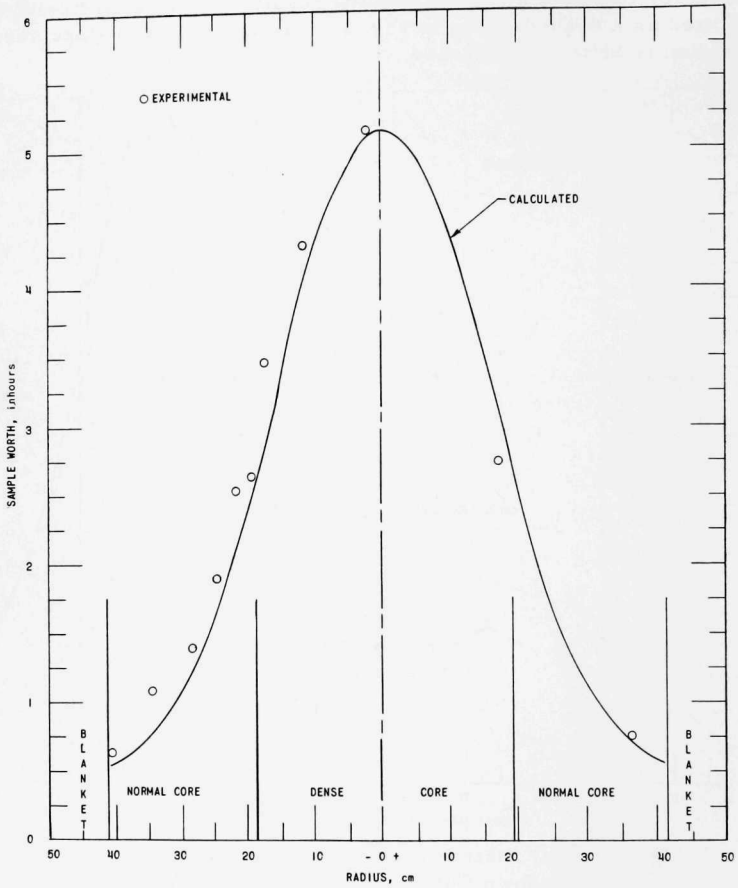

Fig. 4. Radial Danger Coefficient Distribution (Dense Core Sample) for the First Meltdown Configuration

From Figs. 4 and 5, one can see that this configuration should not have a positive coefficient of reactivity, since any expansion of the dense core region would be in the direction of lesser fuel worth and thus lead to a decrease in the reactivity of the system.

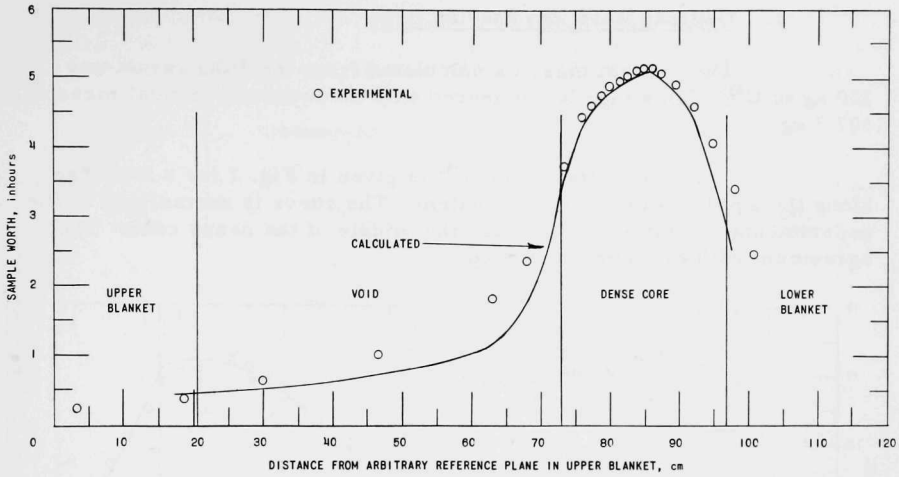

Fig. 5. Axial Danger Coefficient Distribution (Dense Core Sample) for the First Meltdown Configuration

D. Second Meltdown Configuration

1. Description

In the second meltdown configuration, the central portion of the core is assumed to have melted and to have been carried out of the core cavity, after which the outer annular region of the core melts and collapses to form an annular dense core region. The remainder of the core cavity is then left as nearly void.

This configuration was assembled as Assembly No. 28 of ZPR-III. A sketch of the system with its associated dimensions appears in Fig. 6. The compositions of the various regions are as previously given in Table II.

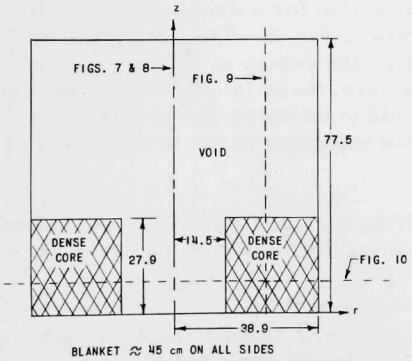

Fig. 6

Second Meltdown Configuration: ZPR-III Assembly No. 28. All Dimensions in Centimeters

2. Critical Mass and Fission Rate

The critical mass as calculated from the PDQ result was 320 kg of U^{235}. This may be compared with an observed critical mass of 307.3 kg.

The rate of fission of U^{235} is given in Fig. 7 for a traverse along the axial centerline of the system. The curve is normalized to the experimental result at a point near the middle of the dense core. The agreement with experiment is good.

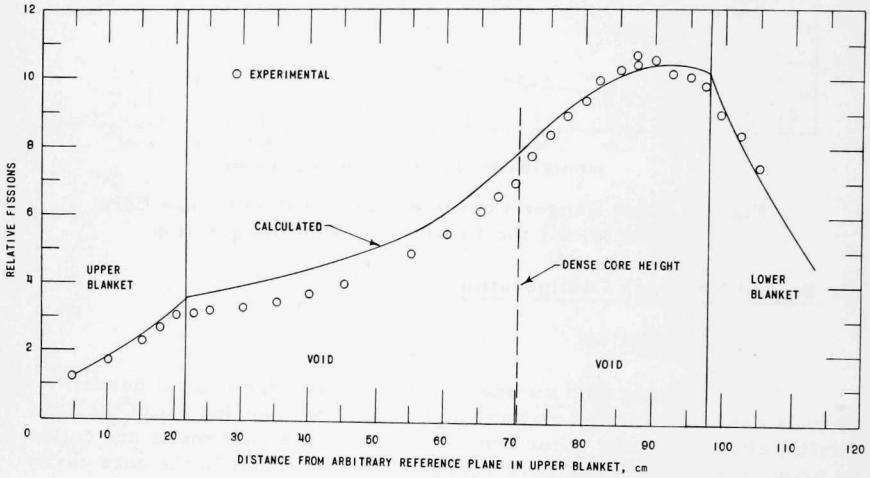

Fig. 7. Axial Distribution of U^{235} Fissions Along Core Centerline for the Second Meltdown Configuration

3. Danger Coefficient Distribution

The danger coefficient distribution for a dense core sample moving along the axial centerline is given in Fig. 8. The normalization is such that a distribution passing through the center of the dense core region agrees with experiment. In this case, there is some disagreement with experiment. The disagreement could possibly be due to either the inadequacy of diffusion theory in the void region or to the crudeness of the two-group cross sections.

It is interesting to note that the worth of a dense core sample on the axial centerline has a minimum near the middle of the dense surrounding band.

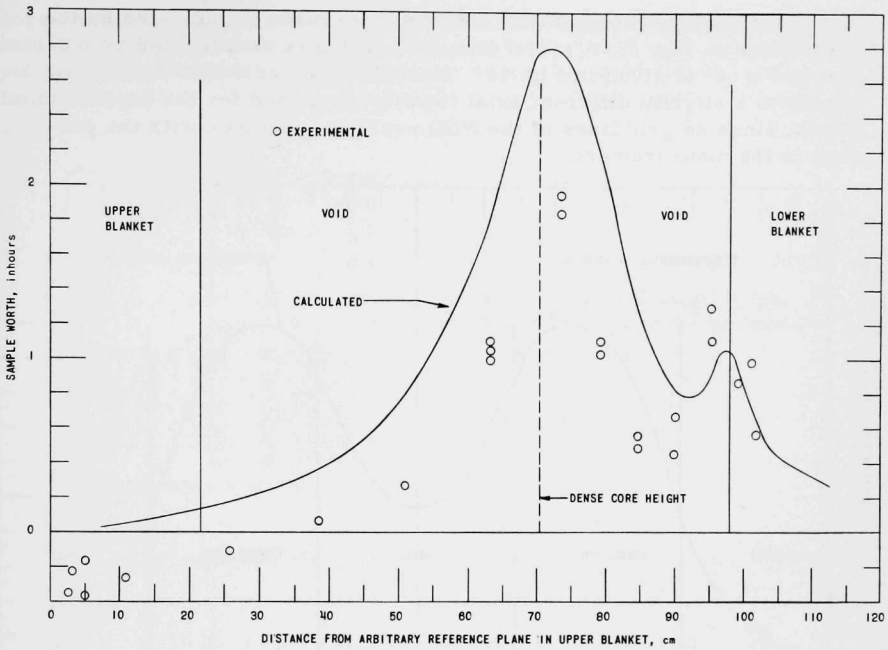

Fig. 8. Axial Danger Coefficient Distribution Along Core Centerline (Dense Core Sample) for the Second Meltdown Configuration

An axial danger coefficient distribution through the dense core region itself is given in Fig. 9.

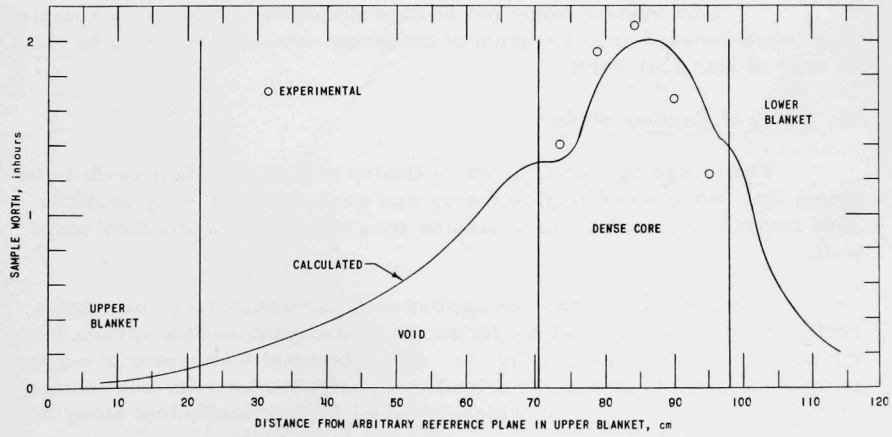

Fig. 9. Axial Danger Coefficient Distribution Through Dense Core (Dense Core Sample) for the Second Meltdown Configuration

The radial position at which the traverse was made is indicated by the dashed line in Fig. 6. A radial traverse, which is also located by a dashed line in Fig. 6, is given in Fig. 10. The calculated curve in Fig. 10 corresponds to a slightly different axial location than used for the experimental points, since no grid lines of the PDQ problem coincided with the position used in the measurement.

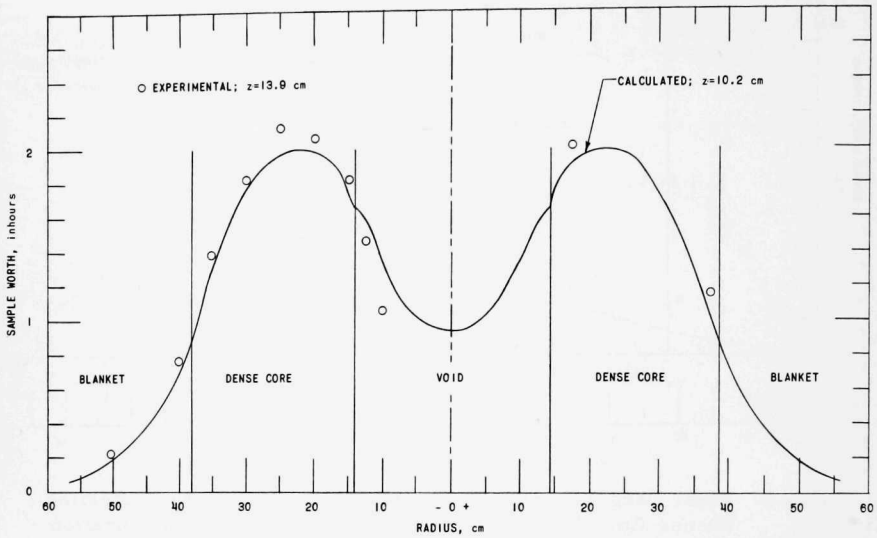

Fig. 10. Radial Danger Coefficient Distribution (Dense Core Sample) for the Second Meltdown Configuration

This system would not be expected to have a positive reactivity coefficient because any expansion of the dense core region would be into an area of less fuel worth.

E. Worth of Further Study

The foregoing comparisons of theory with experiment seem to indicate that two-group diffusion theory and perturbation theory could be used to predict distributions of fission rate and danger coefficient quite well.

The method may thus be applied to study whether or not a given configuration has autocatalytic tendencies. An example of a system leaning this way is presented in Fig. 11. Here the axial component of expansion of the central fuel section could lead to a positive reactivity contribution, as is indicated in Fig. 12, in which the axial danger coefficient along the

core centerline has been plotted. The over-all effect is probably negative because of the small amount of fuel thus involved, and because of the competing effects from other fuel sections. However, more studies remain to be performed.

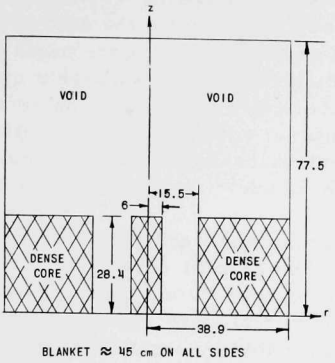

Fig. 11

Third Meltdown Configuration. All Dimensions in Centimeters

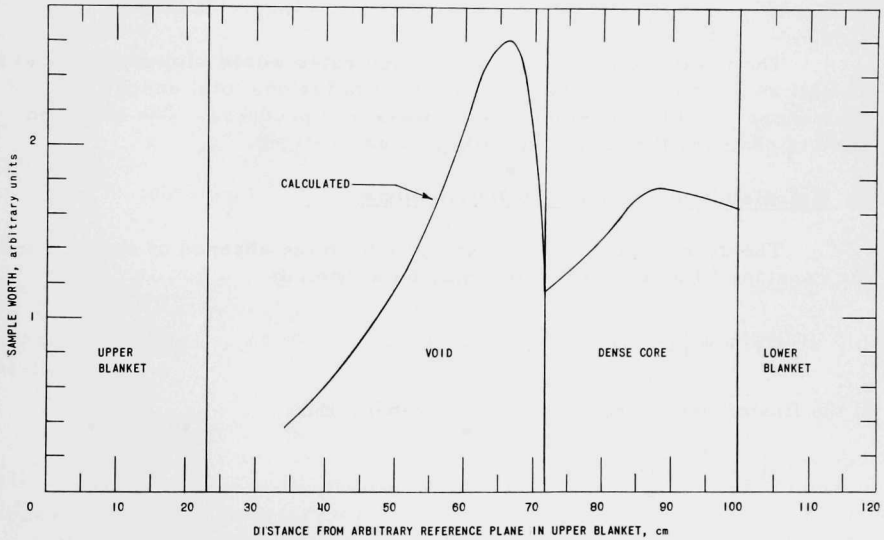

Fig. 12. Axial Danger Coefficient Distribution Along Core Centerline (Dense Core Sample) for the Third Meltdown Configuration

II. EFFECT OF POWER DISTRIBUTION ON YIELD

A. Introduction

There has been some speculation as to how spatial variations of the fission rate in a spherically symmetric core would affect the energy yield in a fast reactor explosion.[7,8] A series of calculations were made to examine this effect. In these, the radial distribution of fissionable material was varied so as to give a variety of parabolically shaped fission rates under controlled conditions of neutron lifetime, core radius, and initial excess reactivity. A series of coupled neutronics-hydrodynamics calculations were then done by means of the AX-I code[9] to study the yield.

The neutronics-hydrodynamics calculations were done with one group of neutrons in spherical geometry. The reactor consisted of a U^{235}-U^{238} core of about 50-liter volume surrounded by a nonfissionable blanket. The distributions of fissionable material were found analytically from diffusion theory and were then approximated by a multiregion version of the AX-I code. In all these calculations, both initial neutron lifetime and core radius were held constant. The initial excess reactivities were chosen to give either a moderate or a relatively severe explosion.

The results are reported for fission rates whose slopes are flat, as well as positive and negative. The results include total energy, excess energy, and the maximum local pressures produced. The effect on yield of changing the blanket density is also reported.

B. Calculation of Enrichment Distributions

The diffusion equation for one group, in the absence of sources and for constant diffusion coefficient, may be written as

$$D\nabla^2\Phi + \left[(\nu - 1)\,\Sigma_f - \Sigma_c\right]\,\Phi = 0 \quad . \tag{5}$$

If the fission rate is required to be parabolic then

$$\Phi\Sigma_f = 1 - \frac{qr^2}{b^2} \quad , \tag{6}$$

where b is the core radius, q is a shape-controlling factor, and the flux level has been chosen to make the fission rate unity at r = 0.

In spherical geometry and for the case of constant capture, substituting (6) into (5) yields an ordinary differential equation of the form

$$\frac{d^2\Phi}{dr^2} + \frac{2}{r}\frac{d\Phi}{dr} + \frac{(\nu - 1)}{D}\left(1 - \frac{qr^2}{b^2}\right) - \frac{\Sigma_c}{D}\,\Phi = 0 \quad . \tag{7}$$

This equation is readily solved by the method of Laplace transforms. The required solution is

$$\Phi(r) = \left[\frac{6(\nu - 1)q}{\Sigma_c \mu^2 b^2} - \frac{(\nu - 1)}{\Sigma_c} + \Phi(0)\right]\frac{\sinh \mu r}{\mu r} - \frac{6(\nu - 1)q}{\Sigma_c \mu^2 b^2} + \frac{(\nu - 1)}{\Sigma_c}\left(1 - \frac{qr^2}{b^2}\right) , \tag{8}$$

where $\mu = (\Sigma_c/D)^{1/2}$ and $\Phi(0)$ is the flux at the center.

The equation for the blanket in the absence of fission is

$$\nabla^2\Phi - \kappa^2\Phi = 0 \tag{9}$$

where

$$\kappa = \left(\frac{\Sigma_c}{D}\right)^{1/2} .$$

The standard solution for this in spherical geometry is easily obtained.

The currents and fluxes for the core and blanket are then equated at the interface to obtain the value of $\Phi(0)$ for criticality:

$$\Phi(0) = \frac{(\nu - 1)}{\Sigma_c}\left\{\frac{\frac{\mu D_r}{D_c}\left[\frac{6}{\mu^2}\frac{q}{b^2} - (1 - q)\right]\left(\kappa \coth \kappa T + \frac{1}{b}\right) + \frac{2q\mu}{b}}{\frac{\mu \cosh \mu b}{b} + \frac{\sinh \mu b}{b}\left[\frac{D_r}{D_c}\left(\kappa \coth \kappa T + \frac{1}{b}\right) - \frac{1}{b}\right]} + 1 - \frac{6q}{\mu^2 b^2}\right\} , \tag{10}$$

where D_c and D_r refer to the diffusion coefficient for core and reflector, and T is the reflector thickness. The macroscopic fission cross section necessary to obtain a parabolic fission rate is then calculated from the relation

$$\Sigma_f(r) = \frac{1}{\Phi(r)}\left(1 - \frac{qr^2}{b^2}\right) . \tag{11}$$

The macroscopic fission cross sections were reduced to relative volume fractions of fissionable material by the relations

$$VF_{25}(r)\ \Sigma_{f25} + VF_{28}(r)\ \Sigma_{f28} = \Sigma_f(r) \tag{12}$$

and

$$VF_{25}(r) + VF_{28}(r) = 1 , \tag{13}$$

where the subscripts 25 and 28 refer to U^{235} and U^{238}, respectively.

The microscopic cross sections which were used throughout are listed in Table III.

Table III

MICROSCOPIC CROSS SECTIONS

	σ_c	$\nu\sigma_f$	ν	σ_s	σ_{tr}
U^{235}	0.2	3.75	2.5	5.3	7.0
U^{238}	0.2	0.25	2.5	6.7	7.0
Blanket Material	0.2	-	-	6.8	7.0

A rough indication of how the enrichment of U^{235} varies from core center to edge is given in Table IV. These values are listed for various values of q and for a core and reflector density of 7.92 g/cc. The core radius was 23.4 cm.

Table IV

U^{235} ENRICHMENT

q	Center	Edge
0	0.34	0.77
0.4	0.43	0.62
0.6	0.48	0.50
0.8	0.55	0.32
-0.2	0.31	0.82
-0.6	0.26	0.90

C. The AX-I Code

The AX-I code treats a spherically symmetric prompt critical system and computes the variation in time and space of the specific energy, pressure, density, and velocity. It also computes the reactivity, power, total energy, and the change of radius as a function of time. Delayed-neutron effects are ignored and no allowance is made for transfer of heat by conduction or radiation.

The input information required includes initial reactivity in the form of inverse period, the initial temperatures of the regions, the parameters for the equation of state, and the microscopic neutron cross sections.

At the outset, the neutronics portion of the program uses the SNG transport code[10] to provide a power distribution and inverse period. After this is finished, the code proceeds to the thermodynamics-hydrodynamics cycle to compute the time variation of power, temperature, pressure density, and material velocity. During a time interval Δt, alpha (the inverse period) is considered to remain constant while the power varies as exp $(\alpha \Delta t)$. The energy is then distributed over the entire system in accord with the previously calculated fission rate. The thermodynamic and hydrodynamic changes are again computed, and then the code tests whether a neutronics calculation should be done or if the power should be allowed to vary exponentially for another increment in time.

In the AX-I code, the relation between pressure and temperature has been taken to be linear, namely,

$$P = \alpha\rho + \beta\theta + \tau \quad ,$$

whereas the specific heat at constant volume is given by

$$\frac{\partial E}{\partial \theta} = A + B\theta \quad ,$$

in which

P = pressure

ρ = density

θ = temperature

E = internal energy .

In order to generate a parabolic power distribution to a reasonable degree of approximation, the AX-I code was modified to allow for up to 39 regions.

D. Preliminary Calculations

The neutronics section of the AX-I code employs the SNG transport code as a subroutine. The SNG code is known to be more reactive[11] than diffusion theory in these core sizes, and in these particular studies the effect was aggravated.* Since the enrichment distribution to give a parabolic power were calculated from diffusion theory, some correction of the data was required to obtain the desired initial excess reactivity and the same neutron lifetime for all the problems in a series, using SNG. It was found that appropriate adjustments in ν, the number of neutrons per fission, and

*D. M. O'Shea, unpublished data.

v, the neutron velocity, for each problem sufficed to meet the desired control of initial conditions. The core radius remained fixed in all cases.

E. The AX-I Calculations

1. Fixed Initial Conditions

The lifetime used for all the AX-I calculations was 0.0209 μsec. The core radius was kept fixed at 23.4 cm. The initial core density was always 7.92 g/cm^3. The constants for the equation of state of core material were

α = 0.02873 cm^2/μsec^2 ;

β = 278.46 g/cm-μsec^2-kev ;

τ = -0.3946 g/cm-μsec^2 ;

A = 12.163 cm^2/μsec^2-kev ;

B = 5780 cm^2/μsec^2-kev^2 .

The initial temperature of the core was θ_i = 1 x 10^{-4} kev. These correspond to a threshold temperature for pressure generation of 6960°K or 6 x 10^{-4} kev.

The constants for the equation of state of the blanket were taken to be the same as in the core with the exception that τ was chosen to make the blanket pressure exactly zero at initial density and temperature. The blanket starting temperature was 5 x 10^{-5} kev.

2. Energy Release and Maximum Pressure

The results of study of a moderate explosion is given in Fig. 13. The initial excess reactivity was 0.000554 δk/k. The solid curves represent results for a blanket density of 7.92 g/cm^3, whereas the dashed curve represents results for a density of 15.84 g/cm^3. The maximum energy release occurs for the case of flat power (q = 0). The lower curves in the figure give the energy available to do work. The available energy is defined to be the total energy minus the energy used in heating the core to threshold temperature. (When the entire core did not reach threshold temperature, the term subtracted was the integral, to threshold, over the actual volume reaching this temperature plus the fission energy developed in the remainder of the core.) For all the power shapes except for q = 0.8, the entire core reached threshold temperature. The effect of doubling the blanket density was to increase the maximum available energy by about 20%.

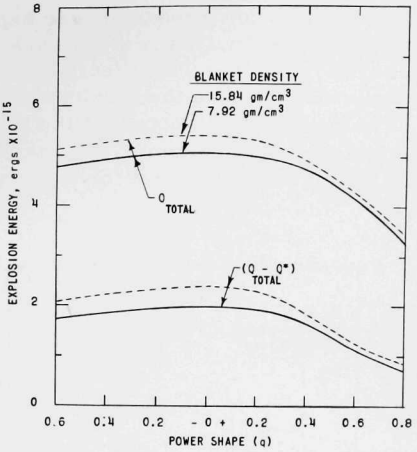

Fig. 13. Explosion Energy vs Power Shape for Power ~ $1 - (qr^2/r_c^2)$; $\ell = 2.09 \times 10^{-8}$ sec; $k_{eff} = 1.000554$; and $r_c = 23.4$ cm

The maximum local pressures calculated are given in Fig. 14. The maximums occur at a positive value of q between 0.2 and 0.4. For positive q, the pressure always peaks at the center of the core; for negative q, the peak occurs away from the center, moving outward as q becomes more negative.

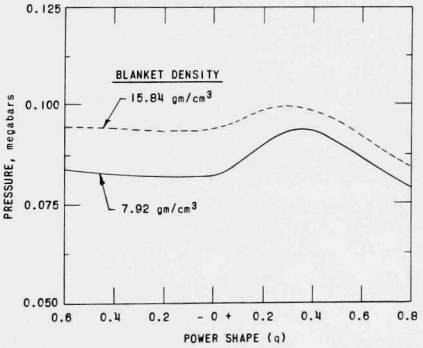

Fig. 14. Maximum Local Pressure vs Power Shape for Power ~ $1 - (qr^2/r_c^2)$; $\ell = 2.09 \times 10^{-8}$ sec; $k_{eff} = 1.000554$; and $r_c = 23.4$ cm

The energy release for a more severe explosion is given in Fig. 15. The initial excess reactivity was 0.004 $\delta k/k$. The maximum total energy release occurs for q = 0.2. The effect of doubling the blanket density is more pronounced here, and the maximum available energy is increased by 33%. It is interesting to note that the yield is not extremely sensitive to the distribution of enrichment. The maximum total energy release is only about 20% greater than that for a uniform distributions of enrichment ($q \approx 0.6$).

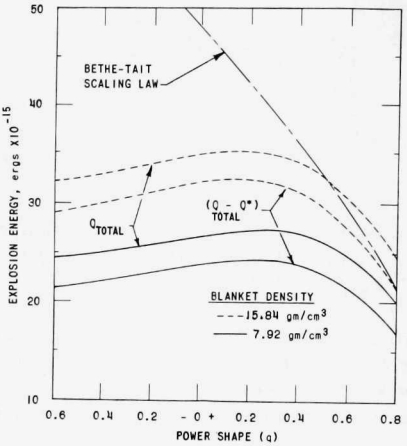

Fig. 15. Explosion Energy vs Power Shape for Power $\sim 1 - (qr^2/r_c^2)$; $\ell = 2.09 \times 10^{-8}$ sec; $k_{eff} = 1.004$; and $r_c = 23.4$ cm

The maximum local pressures produced for the more severe explosions are indicated in Fig. 16.

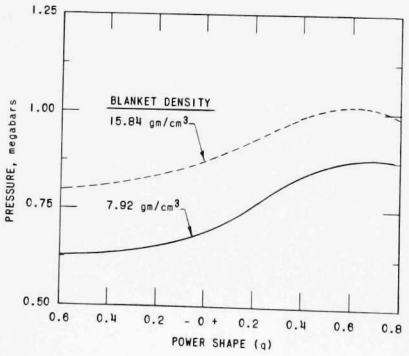

Fig. 16

Maximum Local Pressure vs Power Shape for Power $\sim 1 - (qr^2/r_c^2)$; $\ell = 2.09 \times 10^{-8}$ sec; $k_{eff} = 1.004$; and $r_c = 23.4$ cm

The peak pressures occur for enrichment distributions which are nearly uniform. This is in contrast to the less severe case for which the pressures are maximum at q ~0.3.

These results do not agree with some preliminary conclusions reached by J. H. Tait,[7] who expected that "flattening of the fission rate would reduce the maximum possible energy release and the maximum possible pressures that can be produced."

F. A Bethe-Tait Scaling Law

Bethe and Tait have proposed[8] that the available energy release follows a simple scaling law. If the flux is given by

$$\Phi = 1 - \frac{q_1 r^2}{b^2} \quad ,$$

then the available energy is

$$w \approx \frac{AQ^{*1/2}\lambda_1 b \rho^{1/2}}{(\gamma - 1)^{1/2} q_1^2} \quad .$$

Thus the available energy should be proportional to q_1^2. In the Bethe-Tait derivation, the fission cross section is independent of radius; hence power and flux are synonymous. Since the fission cross section was varied herein, a direct comparison is impossible. However, if one assumes that the "q" dependence in the scaling law relates to the flux, and if the flux shapes corresponding to the various parabolic power distributions used in the AX-I studies is computed, a prediction of sorts can be obtained. The results of this synthetic Bethe-Tait scaling law calculation are plotted on Fig. 15, where the "q" value in the ordinate is the power distribution of the AX-I calculation, not the corresponding flux shape. The Bethe-Tait calculation has been normalized to the AX-I calculation at q = 0.8.

Of course, if the power distribution were inserted into the scaling law, a prediction of infinity would result for q = 0.

One further point of interest relates to the considerable variation of energy yield with blanket density exhibited in Fig. 15. This apparently disagrees with the results obtained by Jankus[12] under the more restrictive condition of no gradient in fission cross section. A full explanation of the differences remains to be given.

III. EFFECT OF DELAYED-NEUTRON FRACTION ON ACCIDENTS

A. Introduction

The EBR-II reactor will be fueled initially with a U^{235}-U^{238} metallic fuel. All of the safety studies made in connection with hazards evaluation of this reactor[13] have used the delayed-neutron fraction appropriate to this mixture (0.754%). However, later fuel charges are expected to include Pu^{239} as a fissionable material, which will lead to sharply reduced delayed-neutron fractions. As a preliminary exploration of the changed safety characteristics for this condition, several startup and fuel-loading accidents, previously calculated[13] for a U^{235}-fueled EBR-II-type reactor, have been recalculated under the assumption that half the original delayed-neutron fraction is present. All other aspects of the reactor behavior were held unchanged. The computing techniques are outlined in some detail in Reference 13 and will not be repeated here.

B. Results

In the calculations for the accidents, it was assumed that reactivity insertion rates ranged from 3×10^{-5} to 0.2 $(\delta k/k)/sec$; yet a general behavior pattern was seen to emerge. The time required for the excursion to reach maximum flux intensity is about halved for the smaller delayed-neutron fraction. The peak fluxes are nearly the same for half the delayed-neutron fraction as for the full value. The integrated fluxes reach nearly the same value for their asymptotes, as they should, since the reactivity feedback coefficients were held unchanged.

It thus appears that no marked changes in reactor safety characteristics are to be expected for the usual loading or startup accident. For the most rapid rates of reactivity insertion considered, the reduced time available for a scram to take effect may be significant; hence, this aspect needs examination. Also, there may be some changes in the temperature rise resulting from the first burst. However, on the whole, the effect of halving the delayed-neutron fraction was not appreciable.

It must be noted that the feedbacks were those appropriate to single-piece, unrestrained metallic pins in a small reactor. The sensitivity to delayed-neutron fraction might be greater in a different set of circumstances.

As an example of the detailed comparison, the results for a hypothetical fuel-loading accident are given in Figs. 17, 18, and 19. If the central fuel element were driven in to a just-critical reactor at a rate of 72 in./min [1.7×10^{-3} $(\delta k/k)/sec$] and all scrams were ineffective, the consequences for an EBR-II-type reactor are presented. The flux is seen to be similar in magnitude and shape for the two delay fractions. The maximum excess reactivity is about half of that with the full delay fraction, but does not fall off so rapidly with time. The integrated fluxes tend toward the same asymptotic value.

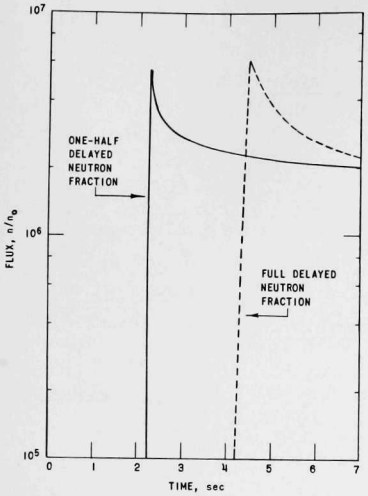

Fig. 17

Flux vs Time. Fuel Element Driven in at 72 in./min [1.7×10^{-3} (δ k/k)/sec]

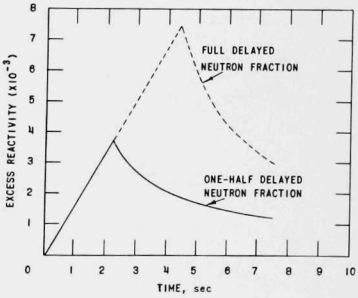

Fig. 18

Excess Reactivity (k_{ex}) vs Time. Fuel Element Driven in at 72 in./min [1.7×10^{-3} (δ k/k)/sec]

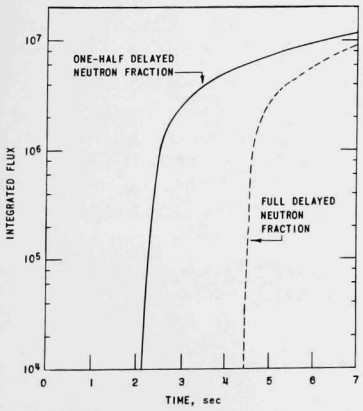

Fig. 19

Integrated Flux vs Time. Fuel Element Driven in at 72 in./min [1.7×10^{-3} (δ k/k)/sec]

REFERENCES

1. W. J. McCarthy, Jr., et al., Studies of Nuclear Accidents in Fast Power Reactors, Proceedings of the Second United Nations Conference on the Peaceful Uses of Atomic Energy, Geneva, Switzerland, 12, 207 (1958).

2. W. Gemmell, Studies of Two Fast Reactor Critical Assemblies Based on Meltdown Configurations, Trans. Am. Nuclear Soc. 3, 335 (Dec 1960).

3. G. G. Bilodeau et al., PDQ - An IBM-704 Code to Solve the Two-dimensional Few-group Neutron-diffusion Equations, WAPD-TM-70 (Aug 1957).

4. B. Carlson, C. Lee, and J. Worlton, The DSN and TDC Neutron Transport Codes, LAMS-2346 (Oct 16, 1959).

5. D. P. Moon, private communication.

6. W. B. Loewenstein and D. Okrent, The Physics of Fast Power Reactors, A Status Report, Proc. of the Second United Nations Conference on the Peaceful Uses of Atomic Energy, Geneva, Switzerland, 12, 16 (1958).

7. J. H. Tait, The Energy Release Caused by a Super-critical Assembly of Fast Reactor Fuel, AERE 7/M146 (April 1957).

8. H. A. Bethe and J. H. Tait, An Estimate of the Order of Magnitude of the Explosion When the Core of a Fast Reactor Collapses, UKAEA-RHM(56)/113 (April 1956).

9. D. Okrent et al., AX-I, A Computing Program for Coupled Neutronics-Hydrodynamics Calculations on the IBM-704, ANL-5977 (May 1959).

10. Bengt G. Carlson, Solution of the Transport Equation by S_n Approximations, LA-1891 (Feb 1955).

11. D. Okrent, R. Avery, and H. H. Hummel, A Survey of the Theoretical and Experimental Aspects of Fast Reactor Physics, Proceedings of the First United Nations International Conference on the Peaceful Uses of Atomic Energy, Geneva, Switzerland, 5, 347 (1955).

12. V. Z. Jankus, A Theoretical Study of Destructive Nuclear Bursts in Fast Power Reactors, ANL-6512 (to be published).

13. L. J. Koch et al., Hazard Summary Report Experimental Breeder Reactor II (EBR-II), ANL-5719 (May 1957).